Journal of The Electrochemical Society



# Material Selection And Optimization Of Conditions For Electrooxidation Of Nitrofurazone: A Comparative Study Of Tin And Lead Dioxides

*Journal of The Electrochemical Society*, 2021 **168** 086507
1945-7111/2021/168(8)/086507/8/$40.00 © 2021 The Electrochemical Society ("ECS"). Published on behalf of ECS by IOP Publishing Limited

# Material Selection And Optimization Of Conditions For Electrooxidation Of Nitrofurazone: A Comparative Study Of Tin And Lead Dioxides

**O. Shmychkova,[1,z] S. Zahorulko,[1] D. Girenko,[1] T. Luk'yanenko,[1] L. Dmitrikova,[2] and A. Velichenko[1]**

[1]*Ukrainian State University of Chemical Technology, Dnipro, Ukraine*
[2]*Dnipro State Medical University, Dnipro, Ukraine*

The electrochemical oxidation of nitrofurazone with $SnO_2$, doped by platinum group metals, and pure $PbO_2$ has been investigated. The oxidation rate of nitrofurazone with $PbO_2$-anode is 5.3 times higher compared to doped $SnO_2$ anodes. It was found that the presence of 1; 2 and 3 g $l^{-1}$ NaCl in electrolyte affects the efficiency of the electrooxidation process in the case of doped $SnO_2$ anodes, the oxidation rate of nitrofurazone increases by 2.3; 3.7; 5.8 times, respectively. Using of doped $SnO_2$ in chloride-containing media allows one to achieve the same rate of destruction of nitrofurazone as when using lead dioxide. Moreover, $SnO_2$ doped electrodes are characterized by the production of a large number of hypochlorous acid and have a higher service life compared to $PbO_2$ in such harsh conditions.
 [DOI: 10.1149/1945-7111/ac1e58]

Manuscript submitted February 25, 2021; revised manuscript received July 31, 2021. Published August 26, 2021.

Supplementary material for this article is available online

The problem of environmental pollution by pharmaceuticals has become acute in recent decades in both developed and developing countries.[1–5] Many different methods have been proposed for wastewater treatment containing drugs, pharmaceuticals and veterinary drugs, which can be classified into destructive (accompanied by the decomposition of pollutants) and non-destructive (without chemical conversion of pollutant). Among them there are traditional treatment methods: biological treatment, filtration and coagulation / flocculation / sedimentation processes, which are one of the most common in practice wastewater disinfection technologies, as well as more modern and advanced methods.[6] Various types of advanced oxidation processes (AOPs) are very effective for disposal and disinfection, although they are not able to provide complete cleaning and must be combined with other treatment methods.[7] In recent years, special attention has been paid to electrochemical methods of disinfection and disinfection of wastewater contaminated with pharmaceuticals.[8,9] Such processes are considered as an attractive alternative to other traditional methods due to the development of new and highly efficient electrode materials and the possibility of their flexible combination with relatively cheap renewable energy sources.[10–13] The last two factors are the main trends in the improvement of existing electrochemical methods of wastewater treatment containing pharmaceutical residues. In this context, the development of conditionally reagent-free electrochemical wastewater treatment methods containing pharmaceutical residues can be extremely effective and attractive.

It is recognized that the efficiency of electrooxidation of organic pollutants depends primarily on the anode material, the nature of the electrolyte, as well as the structure and composition of the toxicant.[14] It is believed[15] that the process of electrooxidation of organic compounds occurs via the mechanism where the secondary transfer of oxygen and adsorbed on the surface of the electrode or free hydroxyl radicals is preferred, rather than direct electron transfer from the compound to the anode. When choosing an electrode material for aqueous solutions, first of all, it is necessary to pay attention to their high mechanical and chemical stability, as well as satisfactory electrical conductivity. In most cases, the anode material must have a high oxygen evolution overvoltage in order to achieve the high selectivity to the target process. Unfortunately, the number of such materials is very limited. Materials based on lead dioxide are recognized as one of the most promising. Their advantage is low cost, manufacturability of creating an active layer, high electrical conductivity and corrosion resistance, especially when polarized at low and medium current densities. Lead dioxide can be relatively easily modified during its electrodeposition in order to improve the electrocatalytic activity and selectivity. Lead dioxide anodes are widely recognized material for electrooxidation of vast organic pollutants.[15,16] However, these electrodes are undergone to significant deterioration in chloride-containing media. In this work we tried to find an alternative material that would not be inferior to lead dioxide in terms of integral activity. Under these conditions, DSA® cannot be used, since in low-concentration chloride media they quickly reach the critical potential of destruction.[17] And materials containing metals of the platinum group or their oxides behave similarly and, as a rule, do not possess their own electrochemical activity in the oxidation of toxic organic substances.[18] The use of BDD results in high cell voltage.[2] In this regard, it is important to the material to have satisfactory stability, electrical conductivity, low cell voltage as well as high selectivity for the electrochemical generation of oxidants capable of effectively destroying contaminants in indirect oxidation. From this point of view, tin and lead dioxides are promising materials. Most of researchers avoid using materials with low oxygen evolution overvoltage in advanced oxidation processes. Nevertheless, there is a practical interest in anodic materials based on $SnO_2$, which is due to their high chemical resistance in both acidic and alkaline solutions and a fairly high electrocatalytic activity in oxygen transfer reactions.[19–21] An additional advantage is that in the presence of chloride ions in solution, such materials are able to create oxidizing agents that take part in secondary oxidation processes. Naked $SnO_2$ is a n-type semiconductor with a band gap of 3.6 eV. It is modified with various electron donors (antimony, fluorine, etc) in order to increase the electrical conductivity.[22–24] However, Sb doped $SnO_2$ undergoes passivation in sulfate and phosphate solutions and has high cell voltage. It is also promising to create composite coatings based on $SnO_2$ and platinum group metal oxides, which are semiconductors with large number of charge carriers.[25] Nevertheless, in terms of their own electrocatalytic activity in the processes of direct electrochemical oxidation, composites based on $SnO_2$ and Pt group metals are significantly inferior to lead dioxide and exhibit high electrocatalytic activity only in chloride-containing media. Yet, tin oxide-based materials, doped with Pd are interesting due to production of high hypochlorous acid amount.

Nitrofurazone was chosen as a model compound; this choice was convenient for us, since the main intermediate products of its

[z]E-mail: lesiandra08@gmail.com

destruction are known.[26] Some nitrofuran derivatives are synthetic chemotherapeutic agents with a broad antimicrobial spectrum. They are active against both Gram-positive and Gram-negative bacteria.[27] The drug is low-toxic; however, high concentrations can cause dyspeptic and neurotoxic effects. Accumulating in natural objects, it has a mutagenic and carcinogenic effect on the human body, which has been confirmed by animal studies.[28] Since the European Union has forbidden the administration of these compounds to food-producing animals[29] with the aim of avoiding harmful effects on human health due to their toxicity, mutagenic and carcinogenic ability, the main focus of researchers was to develop the appropriate technique for the quantification of trace levels of nitrofuran residues.[30] On the one hand, there are a lot of reports concerning the determination of nitrofurazone in different matrices by luminescence, fluorescence, Raman spectroscopy, high-performance liquid chromatography etc.[31] On the other hand, despite a large number of publications, several issues remain to be explained, since there are no reports on the electrooxidation of nitrofurazone, although the collection of electrochemical oxidation signal is more convenient. In addition, the organization of the oxidation process also remains unreported.

## Experimental

All chemicals were reagent grade and were purchased from Sigma-Aldrich. Bidistilled tap water with electrolytic conductivity 1.6 $\mu$S cm$^{-1}$ was used to prepare solutions.

Lead dioxide anodes were prepared according to the standard method described in a number of our publications[32–34] by electrodeposition of $PbO_2$ on a Ti/Pt current collector. Ti sheet was pre-machined, and then degreased in 5 M NaOH at room temperature; and then it was etched in 6 M HCl at 80 °C during 20 min.[32] Platinum layer was deposited catodically at 20 mA cm$^{-2}$ and a temperature of 70 °C from the following electrolyte: 25 g l$^{-1}$ $K_2PtCl_6$; 100 g l$^{-1}$ $NaNO_2$; 10 cm$^3$ of ammonia solution.[35] Under these conditions, the current efficiency of platinum was about 30%. The surface platinum content was 2 mg cm$^{-2}$. The content of deposited platinum was monitored gravimetrically. A solution of the following composition, M: Pb $(CH_3SO_3)_2$–0.1; $CH_3SO_3H$–0.11 was used as the deposition electrolyte. In most cases, the coating was deposited at 4 mA cm$^{-2}$ and 25 °C during 60 min.

$SnO_2$ coatings doped with Pt group metals were pyrolytically applied directly to the titanium surface. It should be noted, that there is a significant oxidation of the titanium surface in the process of forming the first oxide layers. Such process is especially active if the pyrolysis temperature is higher than 450 °C–500 °C. This reduces the adhesion to the surface and increases the transient resistance, which is due to the formation of an oxide layer on the surface of titanium. In this regard, before applying the base coat, 2 layers of $TiO_2$-$PtO_x$ were applied. The intermediate coating solution was prepared by $TiCl_4$ and n-$C_4H_9OH$ mixing in a ratio of 1:4. A solution of $H_2PtCl_6 \times 6H_2O$ in HCl was introduced into the obtained alcoholate. Heat treatment of the first layer was performed for 5 min, and the second for 10 min at a temperature of 400 °C–420 °C. As a base coat, a solution obtained by dissolving an equivalent amount of $SnCl_4$ in n-butanol (5 cm$^3$ of $SnCl_4$ under cooling in 15 cm$^3$ of n-$C_4H_9OH$) was used. Dopants (0.12 g of metallic Pt as $H_2PtCl_6 \times 6H_2O$, and 0.015 g of metallic Pd as $PdCl_2$) were pre-dissolved in HCl before adding to the electrolyte.

The precursor layers were applied with a brush, followed by drying at a temperature of 80 °C–90 °C for 10 min. This was followed by heat treatment in a muffle furnace for 5 min at a temperature of 400 °C–420 °C. After applying 7 layers, heat treatment was performed for 60 min at 500 °C–520 °C. Next, the anode was washed with bidistilled water in an ultrasonic washer, dried at a temperature of 80 °C–90 °C and was polarized in 0.3 M NaCl for 30 min at $j_a = 50$ mA cm$^{-2}$ in order to remove the residues of precursors. The proposed original technique allows one to deposit the compact, homogeneous coatings with high adhesion to the titanium surface. Materials modified with platinum were dark gray, and with palladium they were black.

Anodes surface morphology was studied by scanning electron microscopy (SEM) with Tescan Vega 3 LMU with energy-dispersive X-ray microanalyzer Oxford Instruments Aztec ONE with X-Max$^N$20 detector. X-Ray powder diffraction (XRPD) data were collected in the transmission mode on a STOE STADI P diffractometer with Cu $K\alpha_1$-radiation, curved Ge (1 1 1) monochromator on primary beam, $2\theta/\omega$-scan, angular range for data collection 20.000–110.225 °$2\theta$ with increment 0.015, linear position sensitive detector with step of recording 0.480 °$2\theta$ and times per step 75–300 s, $U$ = 40 kV, $I$ = 35 mA, $T$ = 298 K. A calibration procedure was performed utilizing SRM 640b (Si) and SRM 676 ($Al_2O_3$) NIST standards. Preliminary data processing and X-ray qualitative phase analysis were performed using STOE WinXPOW and PowderCell program packages. Crystal structures of the phases were refined by the Rietveld method with the program FullProf.2k, applying a pseudo-Voigt profile function and isotropic approximation for the atomic displacement parameters, together with quantitative phase analysis.

XPS studies were carried out on a PHI 5000 spectrometer using monochromatic AlK$\alpha$ radiation for excitation. The BE value of C (1s), due to adventitious carbon and residual solvent, is 284.8 (±0.3) eV.

Oxygen evolution reaction was investigated by steady-state polarization and impedance spectroscopy on computer controlled EG & G Princeton Applied Research potentiostat model 273 A and lock-in Amplifier model 5210 in different media (see in Results and Discussion).

Since in the case of using a sulfate solution at high anodic potentials on the surface of electrodes modified with platinum group ions, the formation of persulfates is possible,[36] a phosphate buffer was used as a supporting electrolyte. The electrooxidation of organic compounds was carried out in divided cell at $j_a = 50$ mA cm$^{-2}$. The volume of anolyte was 130 cm$^3$. Solution, containing phosphate buffer (0.25 M $Na_2HPO_4$ + 0.1 M $KH_2PO_4$) + $10^{-4}$ M organic compound, (pH = 6.55) was used as anolyte; phosphate buffer as catholyte. Stainless steel was used as cathode. Doped $SnO_2$ or $PbO_2$ electrodes were used as anodes. Electrode surface area was 2.5 cm$^2$.

The changing of the concentration of the organic substance during the electrolysis was measured by sampling (volume of 5 cm$^3$) at regular intervals and measuring the optical density of the solution in the ultraviolet and visible region (wavelength range 200–350 nm) using a Kontron Uvikon 940 spectrometer.

Analyses of the reaction products were conducted by high performance liquid chromatography (HPLC) using a Shimadzu RF-10A xL instrument equipped with an Ultraviolet SPD-20AV detector and a 30 cm Discovery® C18 column.

## Results and Discussion

***Morphology and physico-chemical properties of materials.***— The morphology and physico-chemical properties of lead dioxide are described in our previous publications in detail.[14,34,35] SEM/EDAX experiments were performed to evaluate the amount and distribution of dopants in $SnO_2$ (see Fig. 1). As one can see, doped $SnO_2$ anode has a slightly porous developed surface. In the porous matrix, probably Pt, there are large well visible inclusions with a size of 20–40 $\mu$m. Palladium is distributed less evenly on the surface: the maximum concentration of palladium is observed in the protruding parts of the surface, and the minimum—in the depressions. Probably these inclusions are the PdO phase, the presence of which in the coating was proved by the X-ray diffraction method (Fig. 2). The parameter of the elementary cubic lattice of Pt is a = 3.9236 Å, the volume V = 60.402 Å$^3$.[37] The parameter of the elementary cubic lattice of Pd is a = 3.8903 Å, the volume V = 58.877 Å$^3$.[38] Since Pt and Pd are isostructural and have similar parameters, their reflexes are superimposed (merged). The closer the lattice parameters (a) are, the less noticeable the XRD reflexes become, which does not allow

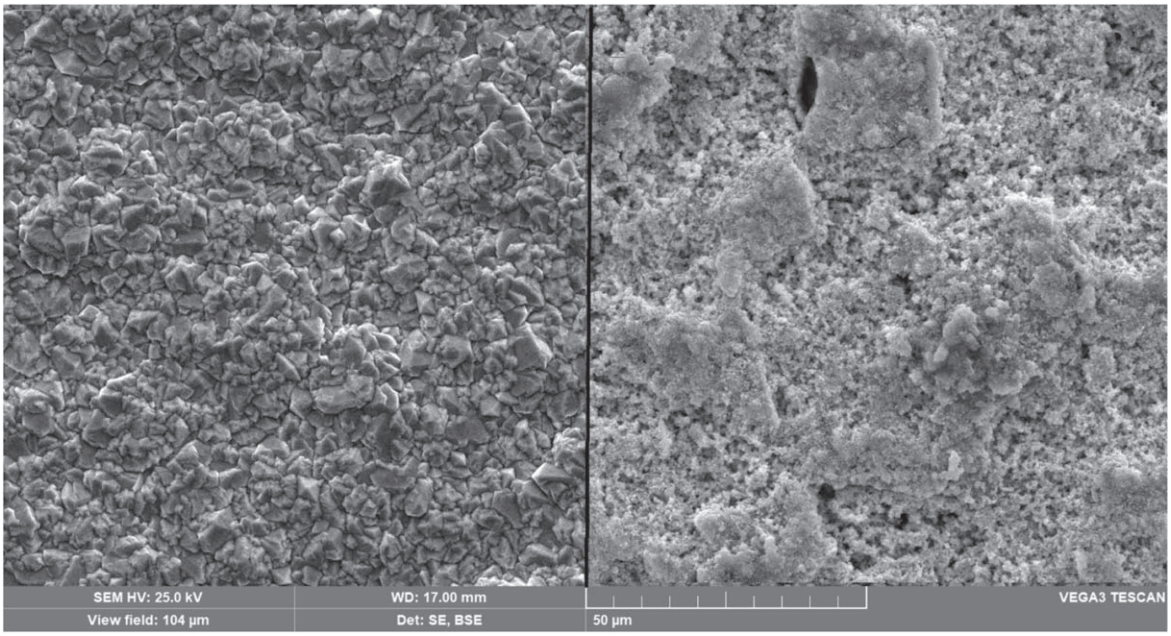


**Figure 1.** SEM micrographs of $PbO_2$ (left); $SnO_2$–8 at.% Pt-12 at.% Pd.

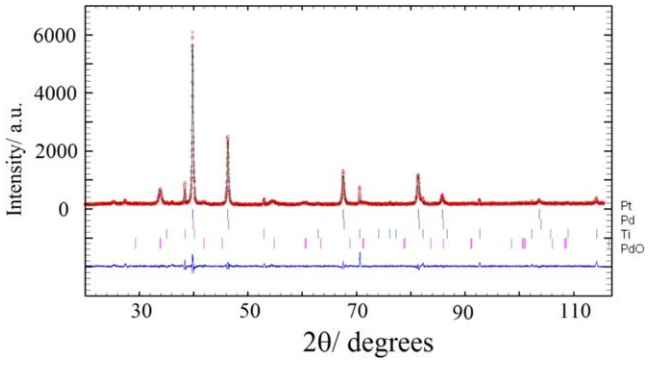


**Figure 2.** Observed and calculated X-ray powder profiles for doped $SnO_2$-electrode. Experimental data (circles) and calculated profile (solid line through the circles) are presented together with the calculated Bragg positions (vertical ticks) and difference curve (bottom solid line).

one to conclude that there are different phases. In our case, the surface content of palladium and platinum is sufficient to separate the reflexes, which allows one to identify the individual phases of platinum and palladium.[39]

According to EDAX analysis (Fig. S1 (available online at stacks.iop.org/JES/168/086507/mmedia)), platinum is evenly distributed on the surface. The distribution of Pd, Sn and Ti coincide with the distribution of oxygen, which indirectly confirms the presence on the surface of the oxides of these elements. This method also identified impurities of $TiO_2$ of rutile and anatase modifications.[40–42]

To get further insight into the effects of doping, we investigated the surface layers by X-ray photoelectron spectroscopy. The XPS spectra of $PbO_2$ have been discussed in detail in our previous publications.[43–45] Works on the XPS characterization of $PbO_2$[46] pointed out the importance of the examination of O1s region as it provides information on the hydration state of the surface. In particular Bi causes a very high hydroxylation with respect to $PbO_2$ stoichiometry.[46]

As one can see from the obtained photoelectron spectra of doped $SnO_2$ sample (Fig. 3), there is titanium on the surface, most likely in the form of oxide. Titanium appears on the surface as a result of thermal diffusion from the surface of titanium during heat treatment of the anode.

Some tin content is recorded in the surface layer. Tin alcoholate, which is used as the main precursor, is able to partially sublimate from the surface to thermal decomposition, without participating in the formation of the $SnO_2$ matrix. This is the main problem of obtaining reproducible coatings based on $SnO_2$.

The content of elements in the surface layer 4–5 nm thick was calculated for the obtained anodes. The surface ratio of Pt, Pd with the ratio of elements in precursors is quite close. Tin in the coating is present in a concentration of 6.7 at.%, and Ti in small quantities (3.8 at.%). The collected spectra show three peaks in the O 1 s region: the one at the lower binding energy was assigned to strongly bounded lattice oxygen of $PdO_x/PtO_x/SnO_x$, while the broader one at higher binding energy was attributed to weakly bound oxygen species: adsorbed $OH^-$ at 531.2 eV and water at 533.8 eV,[45,46] that means interaction with water in outer regions (see Fig. 3, O 1s core level), since such binding energy is too high for the oxide-hydroxide compounds of metals.[47] The integrated area of O1s peaks assigned to labile oxygen-containing particles are significantly higher in this spectrum compared to peak of inert particles, which indicates a high surface content of water adsorbed on the active clusters in the amorphous zone of the oxide surface.[48] We assumed that palladium oxides are the main centers of water adsorption, and their presence in the coating contributes to the hydroxylation of the anode surface. Most likely, this property of palladium compounds provides its high electrocatalytic activity in the reaction of formation of hypochlorite, which involves oxygen-containing particles with low bond strength.

***Electrocatalytic properties of materials.—*** *The oxygen evolution reaction.*—The next step of our work was to evaluate the electrocatalytic activity of materials in oxygen transfer reactions. It is now well recognized[49] that, in the direct electrolysis process, the oxidation of a large number of organic and inorganic compounds on different electrode materials, including $PbO_2$ and $SnO_2$, proceeds simultaneously with the evolution of oxygen. Highly oxidizing oxygen species, such as OH radicals, formed during the anodic oxidation of water are able, in turn, to oxidize most of organic compounds.

The rate of the oxygen evolution reaction can vary depending on the nature and amount of the dopant.[42,44,50] The change in the

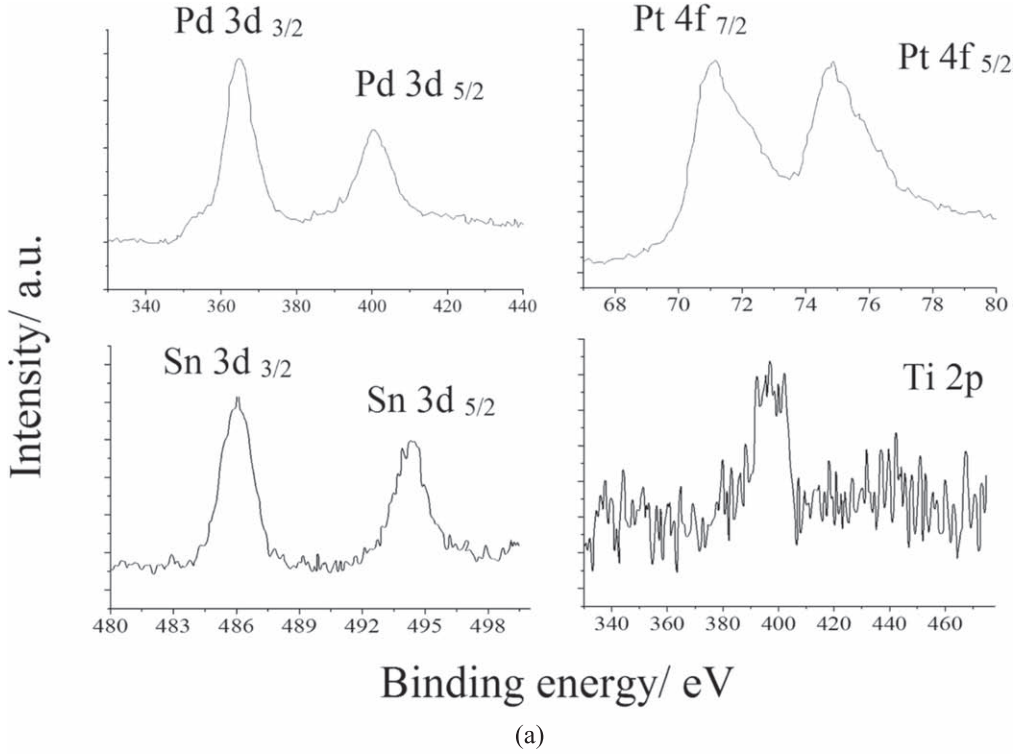


(a)

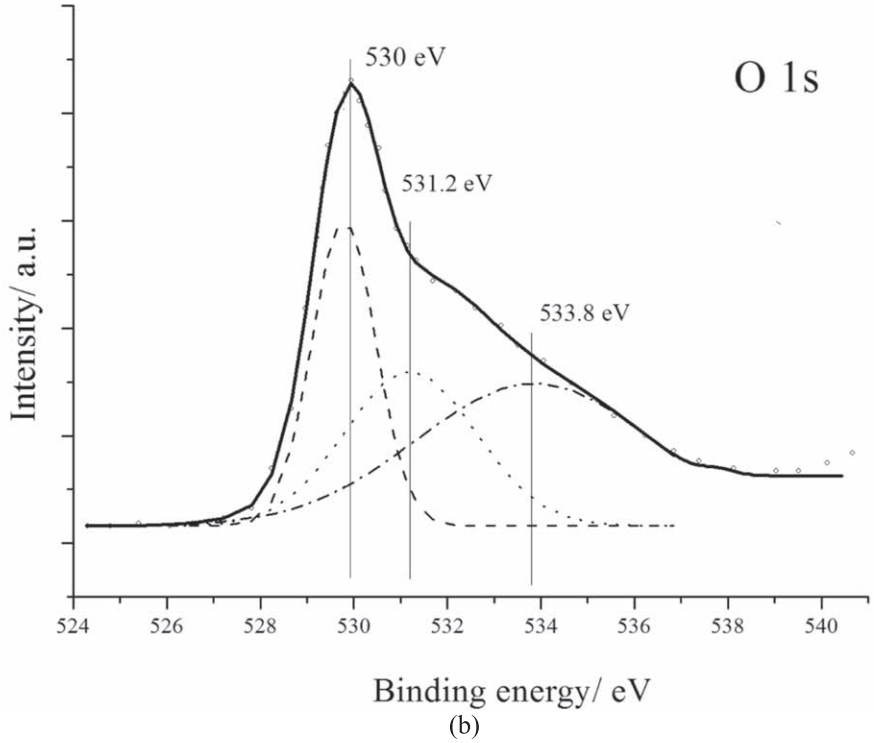


(b)

**Figure 3.** Pd 3d, Sn 3d, Pt 4f, Ti 2p core levels (a) and modeled O 1s level (b) structures in $SnO_2$–8 at.% Pt-12 at.% Pd.

properties of modified coatings in the oxygen evolution reaction mainly depends on the change in the chemical properties of the oxide surface, which in turn leads to a change in the bond strength of oxygen-containing particles chemisorbed on the electrode surface.

The regularities of the reaction of oxygen evolution on $PbO_2$ can be satisfactorily explained within the framework of the mechanism proposed by Pavlov et al.[51]

$$PbO\cdot(OH)_2 + H_2O \rightarrow PbO\cdot(OH)_2\ldots(OH^{\cdot}) + H^+ + e^- \quad [1]$$

$$PbO\cdot(OH)_2\ldots(OH^{\cdot}) \rightarrow PbO\cdot(OH)_2 + O + H^+ + e^- \quad [2]$$

$$2\,O \rightarrow O_2 \quad [3]$$

According to,[51] if the oxygen evolution reaction is limited by the second electron transfer stage (electrochemical desorption), an increase in the bond strength of chemisorbed oxygen will lead to an increase in the oxygen evolution overvoltage. Under conditions when the transfer of the first electron (electrochemical adsorption) is the limiting stage, the overvoltage of the oxygen evolution reaction will decrease.

Oxygen evolution was studied in buffer instead of perchloric acid in order to get further insight in simultaneous processes of oxygen evolution and oxidation of organic compound in the same media.

As one can see from obtained results (Fig. 4), the oxygen evolution potential on doped $SnO_2$ is significantly lower than on $PbO_2$. The value is 1.1 and 1.7 V for $SnO_2$ and $PbO_2$, respectively. All polarization curves are linear in semi-logarithmic coordinates, and have a tafel slope 110 mV for $SnO_2$ and 190 mV (in phosphate buffer) for $PbO_2$, respectively. Such a small slope for doped $SnO_2$ indicates a drop in transfer of the first electron in the formation of adsorbed oxygen-containing $OH_{ads}$ particles. Obtained data are satisfactorily agreed with the results of photoelectron spectroscopy for the O 1 s region, where the strongly bounded lattice oxygen is high for tin dioxide-based materials.

*Oxidation of nitrofurazone.*—The initial spectrum of the nitrofurazone solution is characterized by two absorption maxima at 260 and 380 nm (Fig. 5).

Nitrofurazone shows rapid isomerization by the C-N double bond to the syn-form, with a shift of the main peak from 380 to 370 nm during electrooxidation. This phenomenon is consistent with the data of De Luca et al.,[52] which showed the presence of the syn-isomer in solution during the photolysis of nitrofurazone. Afterwards one can see a decrease in the optical density of absorption maxima, and the sequential formation of 5-nitro-2-furaldehyde 5-nitro-2-furoic acid as intermediate oxidation products at 310–320 nm after 5 h of electrolysis, which formation were detected by high performance liquid chromatography method (Fig. S2). These results coincide with the data obtained by Nakamura et al.[53] during aqueous chlorination of initial compound. It is interesting to note that the rate of destruction of 5-nitro-furaldehyde is significantly lower than the rate of destruction of 5-nitro-furoic acid. Further oxidation leads to the disappearance of peaks at 260 and 380 nm and the lack of absorption in the range of 310–320 nm, which indicates the complete conversion of nirtofurazone and aromatic products of its oxidation to aliphatic acids after 9 h of electrolysis.

Plot of concentration of the initial compound versus electrolysis time indicates the zero-order reaction (Fig. 5, inset) and considering the catalytic nature of the destruction of nitrofurazone. A heterogeneous rate constant of nitrofurazone destruction was calculated, the value of which is $1.92 \times 10^{-7}$ mol $l^{-1}$ $min^{-1}$.

On the opposite, spectral data showed that the complete conversion of nitrofurazone to aliphatic products at lead dioxide anodes occurs in approximately 2 h (Fig. 6).

The spectrum of initial solution is characterized by absorption maxima at 260 and 380 nm. A decrease in the optical density of the absorption and decolorization maxima was observed during electrolysis. In this case, the intermediate oxidation product 5-nitro-2-furoic acid does not accumulate, but is immediately oxidized.

The oxidation of nitrofurazone on $PbO_2$ anode can also be described by the kinetic equation of zero-order reaction, which indicates a significant role of the adsorption stage of the heterogeneous catalytic process. A heterogeneous rate constant of nitrofurazone destruction was calculated, the value of which is $1.02 \times 10^{-6}$ mol $l^{-1}$ $min^{-1}$.

As one can see, the rate oxidation of nitrofurazone on lead dioxide is 5.3 times higher than on Pt, Pd-doped $SnO_2$. It is obvious that the slow oxidation of the pollutant on $SnO_2$ anodes is associated with the accumulation of 5-nitro-2-furaldehyde, the destruction of which requires much more electrolysis time, in contrast to $PbO_2$ anodes, in which case the intermediate product is immediately oxidized.

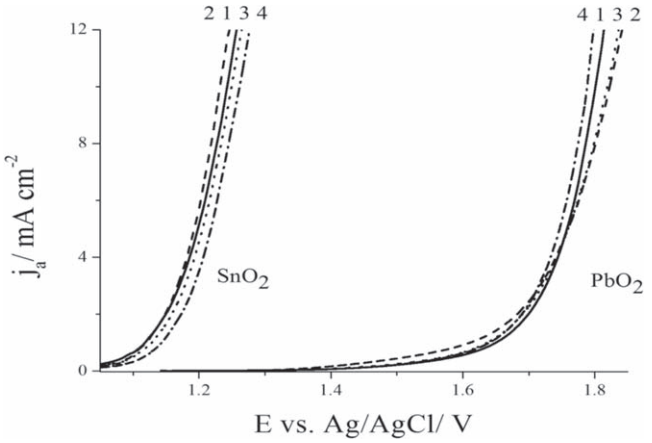


**Figure 4.** Steady state polarization curves of oxygen evolution in different media (Scan rate 1 mV $s^{-1}$, t = 25 °C) on doped $SnO_2$ and $PbO_2$-electrodes, where 1 was recorded in buffer solution; 2–in buffer with 3 g $l^{-1}$ NaCl; 3–in buffer solution with 0.1 mM nitrofurazone; 4–in buffer solution with 0.1 mM nitrofurazone and 3 g $l^{-1}$ NaCl. Coatings were deposited on Ti/Pt sheet.

According to results, obtained by UV-spectroscopy and high-performance liquid chromatography, we propose the probable mechanism of nitrofurazone electrooxidation (Fig. 7).

*Oxidation of nitrofurazone in the presence of chloride-ions.*—The presence of sodium chloride in hospital effluents is a positive aspect because it improves electrical conductivity and is involved in the generation of oxygen-containing chlorine compounds, such as $ClO^-$, HClO, formed during electrolysis and involved in chemical reactions of indirect oxidative destruction of nitrofurazone.

Initial spectra of nitrofurazone solutions with 1–3 g $l^{-1}$ NaCl are characterized by absorption maxima at 260 and 380 nm (not shown). There is a decrease in the optical density of the absorption maxima, and the formation of 5-nitro-2-furaldehyde, as evidenced by the appearance of a peak at 320 nm. 3, 2 and 1.33 h are needed for maximum accumulation of 5-nitro-2-furaldehyde; 4, 2.5 and 1.67 h are needed for the disappearance of the peak at 380 nm, when 1; 2; and 3 g $l^{-1}$ $Cl^-$ are added to the initial solution, respectively. The disappearance of absorption maxima at 260, 320 nm after 7; 5 and 2.5 h, respectively, indicates the complete degradation of nitrofurazone.

The nature of the concentration versus time plot indicates the zero order of the reaction (Fig. 8).

Heterogeneous rate constants of nitrofurazone degradation in solutions with different concentrations of chloride ions were calculated, the data are shown in the Table I.

The $SnO_2$-based coating doped with both palladium (12 at.%) and platinum (8 at.%) is the optimal electrocatalyst for the synthesis of sodium hypochlorite.[54] Therefore, there is an acceleration of the rate of nitrofurazone destruction, due to the formation of hypochlorite and hypochlorous acid with increasing concentration of chloride ions in the solution.

The obtained results showed that the destruction time of nitrofurazone is 1.3 h on $PbO_2$ anodes, regardless of the amount of sodium chloride in the solution. The nature of the concentration versus time plot indicates the zero order of the reaction; the value of the heterogeneous rate constant in the presence of NaCl is $1.14 \times 10^{-6}$ mol $l^{-1}$ $min^{-1}$.

The processes of electrooxidation of nitrofurazone on lead dioxide anodes without and in the presence of 1–3 g $l^{-1}$ NaCl are qualitatively the same. The oxidation rate of initial compound in the presence of NaCl is 1.12 times higher compared to pure buffer without chloride-ions. In addition, the rate of $OCl^-$ generation remained constant under the experimental conditions. Most likely, hypochlorite is developed very slowly and does not significantly affect the rate of this reaction. Therefore, one can assume that the

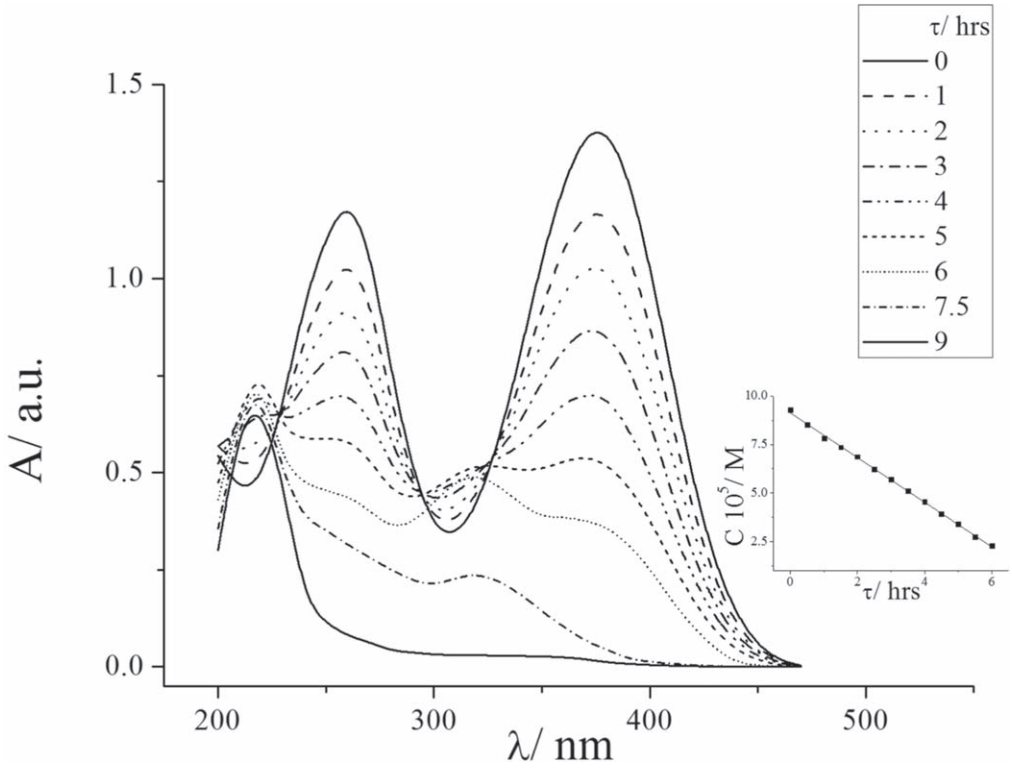


**Figure 5.** Electronic absorption spectra of solutions with 0.1 mM initial concentration of nitrofurazone during electrolysis on Pt, Pd-doped $SnO_2$ anode at 50 mA $cm^{-2}$. Inset: concentration of nitrofurazone versus electrolysis time.

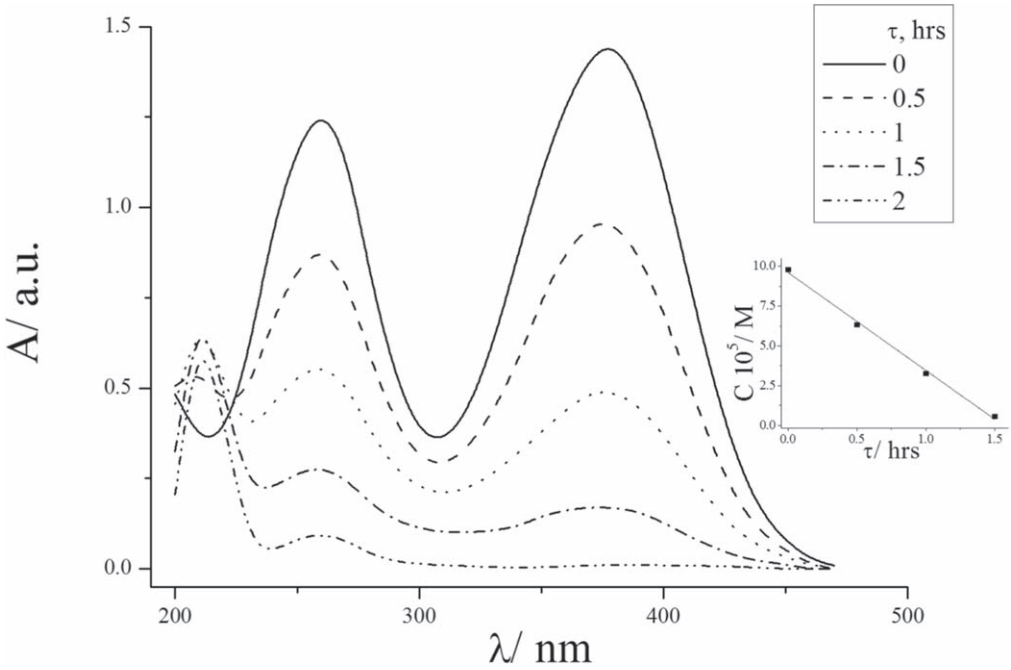


**Figure 6.** Electronic absorption spectra of 0.1 mM solutions of nitrofurazone during electrolysis on $PbO_2$ anode at 50 mA $cm^{-2}$.

presence of chloride ions in the solution does not significantly affect the rate of oxidation of nitrofurazone during the electrolysis on lead dioxide.

Analysis of the data obtained (see Fig. 4) shows that the oxygen evolution and the oxidation of organic compounds (in particular nitrofurazone) occur through the same type of intermediate oxygen-containing particles. There is a clear inhibition of oxygen evolution on $SnO_2$ in the presence of both organic compound and $Cl^-$ ions in the solution. No one sees contribution from direct organic oxidation. Nitrofurazone is removed more efficiently on $PbO_2$ due to high number of oxygen-containing particles, strongly bounded to the oxide surface, which is typical for lead dioxide.[46,55]

It should be noted, that in the presence of 3 g $l^{-1}$ of chloride in the electrolyte, the largest amount of $OCl^-$ involved in secondary oxidative processes is produced on doped $SnO_2$, which allows one to achieve the total rate of the process, the same as when using a $PbO_2$

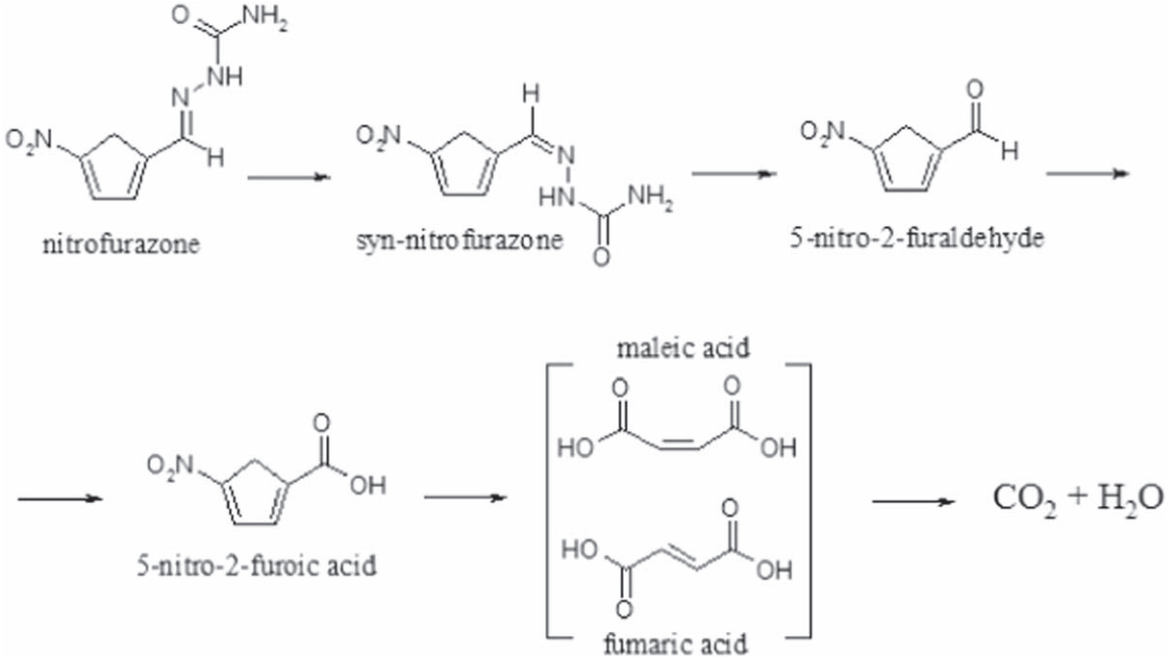


**Figure 7.** Scheme of electrooxidation pathway of nitrofurazone.

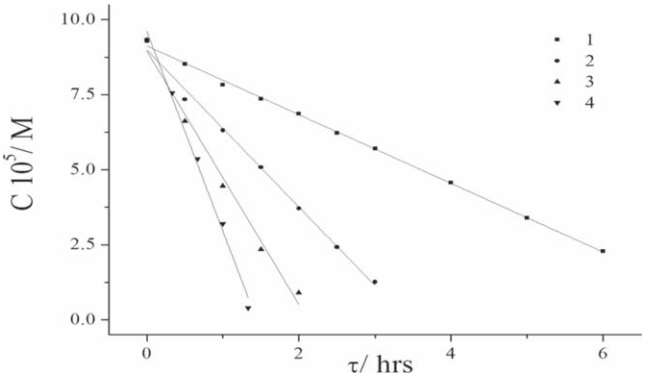


**Figure 8.** Concentration of nitrofurazone versus time of electrolysis in phosphate buffer in the presence of X g $l^{-1}$ NaCl, where 1 is 0; 2–1; 3–2; 3–3.

**Table I. Heterogeneous rate constants of nitrofurazone oxidation in the presence of chloride-ions in the solution.**

| $C_{NaCl}$, g $l^{-1}$ | k × $10^7$, mol $l^{-1}$ $min^{-1}$ |
|---|---|
| 0 | 1.92 |
| 1 | 4.36 |
| 2 | 7.04 |
| 3 | 11.1 |

anode, which can be interesting in terms of using such materials for wastewater disinfection.

## Conclusions

It was revealed that the oxidation rate of nitrofurazone with $PbO_2$-anode is 5.3 times higher compared to $SnO_2$ anodes doped with platinum group metals. In terms of their own electrocatalytic activity in the processes of direct electrochemical oxidation, composites based on $SnO_2$ and Pt group metals are significantly inferior to lead dioxide and exhibit high electrocatalytic activity only in chloride-containing media. It was found that the presence of 1; 2 and 3 g $l^{-1}$ NaCl in electrolyte affects the efficiency of the electrooxidation process in the case of using doped $SnO_2$ anodes, the oxidation rate of nitrofurazone increases by 2.3; 3.7; 5.8 times, respectively. Whereas in the case lead dioxide anodes, the rate of destruction is almost unchanged, regardless of the number of chloride ions in solution.

According to the X-ray diffraction analysis results, palladium in the heat-treated electrocatalytic tin dioxide-based coating Ti/$SnO_2$-Pt-Pd is in the form of a $PdO_x$ phase. X-ray photoelectron spectroscopy has shown that the surface of $PdO_x$ has a high affinity for hydroxylation—adsorption of $H_2O$ and $OH^-$, and their surface content is proportional to the concentration of palladium in the coating.

It has been shown that $SnO_2$ electrodes modified with platinum group metals in media containing chloride ions are characterized by the production of a large number of chloro- and oxygen-containing oxidants (hypochlorous acid) and have a higher service life compared to $PbO_2$, so the use of such materials in chlorine-containing wastewaters will allow not only direct electrooxidation of organic pollutants, but also disinfection simultaneously.

## Funding

This work was supported by National Research Foundation of Ukraine [grant number 2020.01/0015, 2020].

## ORCID

O. Shmychkova https://orcid.org/0000-0001-9490-9706
A. Velichenko https://orcid.org/0000-0003-1076-9991

## References

1. L. Feng, E. D. van Hullebusch, M. A. Rodrigo, G. Esposito, and M. A. Oturan, *Chem. Eng. J.*, **228**, 944 (2013).
2. M. A. Oturan, *Curr. Opin. Solid State Mater. Sci.*, **25**, 100925 (2021).
3. C. A. Martinez-Huitle and M. Panizza, *Curr. Opin. Electrochem.*, **11**, 62 (2018).
4. C. A. Martinez-Huitle and E. Brillas, *Appl. Catal. B*, **87**, 105 (2009).
5. E. Brillas and C. A. Martinez-Huitle, *Appl. Catal. B*, **166–167**, 603 (2015).
6. S. O. Ganiyu, C. A. Martinez-Huitle, and M. A. Oturan, *Curr. Opin. Electrochem.*, **27**, 100678 (2021).
7. E. T. Anthony, M. O. Ojemaye, O. O. Okoh, and A. I. Okoh, *Environ. Pollut.*, **263**, 113791 (2020).
8. I. Sires and E. Brillas, *Curr. Opin. Electrochem.*, **40**, 212 (2021).

9. C. A. Martinez-Huitle and S. Ferro, *Chem. Soc. Rev.*, **35**, 1324 (2006).
10. S. O. Ganiyu, C. A. Martinez-Huitle, and M. A. Rodrigo, *Appl. Catal. B*, **270**, 118857 (2020).
11. Z. Hu, J. Cai, G. Song, Y. Tian, and M. Zhou, *Curr. Opin. Electrochem.*, **26**, 100659 (2021).
12. G. R. Salazar-Banda, G. O. S. Santos, I. M. D. Gonzaga, A. R. Doria, and K. I. B. Eguiluz, *Curr. Opin. Electrochem.*, **26**, 100663 (2021).
13. S. O. Ganiyu and C. A. Martinez-Huitle, *Curr. Opin. Electrochem.*, **22**, 211 (2021).
14. O. Shmychkova, T. Luk'yanenko, L. Dmirtikova, and A. Velichenko, *J. Serbian Chem. Soc.*, **84**, 187 (2019).
15. R. Vargas, C. Borras, D. Mendez, J. Mostany, and B. R. Scharifker, *J. Solid State Electrochem.*, **20**, 875 (2016).
16. X. Li, D. Pletcher, and F. C. Walsh, *Chem. Soc. Rev.*, **40**, 3879 (2011).
17. C. R. Costa, F. Montilla, E. Morallon, and P. Olivi, *J. Hazard. Mater.*, **180**, 429 (2010).
18. G. V. Fortunato, E. S. F. Cardoso, B. K. Martini, and G. Maia, *Chem. Electro. Chem.*, **7**, 1610 (2020).
19. P. Yao, X. Chen, H. Wu, and D. Wang, *Surf. Coat. Tech.*, **202**, 3850 (2008).
20. R. J. Watts, D. D. Finn, M. S. Wyeth, and A. L. Teel, *Water Environ. Res.*, **80**, 490 (2008).
21. F. Li, Q. Liu, J. Hu, J. Yang, and J. Ma, *J. Phys. D*, **53**, 353001 (2020).
22. J. E. L. Santos, D. C. de Moura, M. Cerro-Lopez, M. A. Quiroz, and C. A. Martinez-Huitle, *J. Electroanal. Chem.*, **873**, 114438 (2020).
23. N. Bravo-Yumi, P. Espinoza-Montero, A. Picos-Benitez, R. Navarro-Mendoza, E. Brillas, and J. M. Peralta-Hernandez, *Electrochim. Acta*, **358**, 136904 (2020).
24. G. O. S. Santos, A. R. Doria, V. M. Vasconcelos, C. Saez, M. A. Rodrigo, K. I. B. Eguiluz, and G. R. Salazar-Banda, *Chemosphere*, **259**, 127475 (2020).
25. M. G. Fernandez-Aguirre, R. Berenguer, S. Beaumont, M. Nuez, A. La Rosa-Toro, J. M. Peralta-Hernandez, and E. Morallon, *Electrochim. Acta*, **354**, 136686 (2020).
26. Y. Hou, G. Huan, S. Wang, Z. Yu, S. Qin, L. Tu, Y. Yan, X. Chen, H. Zhu, and Y. Tan, *J. Hazard. Mater.*, **384**, 121438 (2020).
27. T. Delatour, E. Gremaud, P. Mottier, J. Richoz, F. A. Vera, and R. H. Stadler, *J. Agric. Food Chem.*, **51**, 6371 (2003).
28. L. Charuaud, E. Jarde, A. Jaffrezic, M.-F. Thomas, and B. Le Bot, *J. Hazard. Mater.*, **361**, 169 (2019).
29. A. Guzman, L. Agui, M. Pedrero, P. Yanez-Sedeno, and J. M. Pingarron, *Electroanalysis*, **16**, 1763 (2004).
30. M. S. da Silva Juliao, E. C. Almeida, M. A. La Scalea, N. G. Ferreira, R. G. Compton, and S. H. P. Serrano, *Electroanalysis*, **17**, 269 (2005).
31. T. Gan, J. Li, L. Xu, Y. Yao, and Y. Liu, *J. Electroanal. Chem.*, **848**, 113287 (2019).
32. A. Velichenko, T. Luk'yanenko, and O. Shmychkova, *J. Energy Storage*, **30**, 101581 (2020).
33. V. Knysh, T. Luk'yanenko, O. Shmychkova, R. Amadelli, and A. Velichenko, *J. Solid State Electrochem.*, **21**, 537 (2017).
34. O. Shmychkova, T. Luk'yanenko, A. Piletska, A. Velichenko, R. Gladyshevskii, P. Demchenko, and R. Amadelli, *J. Electroanal. Chem.*, **746**, 57 (2015).
35. O. Shmychkova, T. Luk'yanenko, A. Yakubenko, R. Amadelli, and A. Velichenko, *Appl. Catal. B*, **162**, 346 (2015).
36. L. W. Matzek and K. E. Carter, *Chemosphere*, **151**, 178 (2016).
37. J. W. Arblaster, *Platinum Metals Rev.*, **41**, 12 (1997).
38. J. W. Arblaster, *Platinum Metals Rev.*, **56**, 181 (2012).
39. K. Sakurai and M. Mizusawa, *Anal. Chem.*, **82**, 3519 (2010).
40. D. A. H. Hanaor and C. C. Sorrell, *J. Mater. Sci.*, **46**, 855 (2011).
41. A. R. Khataee, H. Aleboyeh, and A. Aleboyeh, *J. Exp. Nanosci.*, **4**, 121 (2009).
42. E. J. Mittemeijer and P. Scardi, *Diffraction analysis of the microstructure of materials* 549(Springer, Berlin) (2004).
43. O. Shmychkova, T. Luk'yanenko, A. Velichenko, L. Meda, and R. Amadelli, *Electrochim. Acta*, **111**, 332 (2013).
44. O. Shmychkova, T. Luk'yanenko, A. Velichenko, and R. Amadelli, *J. Electroanal. Chem.*, **706**, 86 (2013).
45. O. Shmychkova, T. Luk'yanenko, R. Amadelli, and A. Velichenko, *J. Electroanal. Chem.*, **717–718**, 196 (2014).
46. R. Amadelli, L. Armelao, E. Tondello, S. Daolio, M. Fabrizio, C. Pagura, and A. Velichenko, *Appl. Surf. Sci.*, **142**, 200 (1999).
47. J. F. Moulder, W. F. Stickle, P. E. Sobol, and K. D. Bomben, *Handbook of X-ray Photoelectron Spectroscopy, Physical Electronics* (Perkin-Elmer Corporation) (Eden Prairie, Minnesota, USA) (1995).
48. P. Ruetschi and R. Giovanoli, *Power Sources*, **13**, 81 (1991).
49. S. Trasatti, *Electrochim. Acta*, **45**, 2377 (2000).
50. A. Velichenko, T. Luk'yanenko, N. Nikolenko, O. Shmychkova, P. Demchenko, and R. Gladyshevskii, *J. Electrochem. Soc.*, **167**, 063501 (2020).
51. D. Pavlov, B. Monahov, and D. Petrov, *J. Power Sources*, **85**, 59 (2000).
52. M. De Luca, S. Mas, G. Ioele, F. Oliverio, G. Ragno, and R. Tauler, *Int. J. Pharm.*, **386**, 99 (2010).
53. H. Nakamura, T. Kawakami, T. Niino, Y. Takahashi, and S. Onodera, *J. Toxicol. Sci.*, **33**, 621 (2008).
54. D. V. Girenko and A. B. Velichenko, *Surf. Eng. Appl. Electrochem.*, **54**, 88 (2018).
55. O. Shmychkova, T. Luk'yanenko, R. Amadelli, and A. Velichenko, *J. Electroanal. Chem.*, **774**, 88 (2016).